SolarPACES 2022, 28th International Conference on Concentrating Solar Power and Chemical Energy Systems
Thermal Energy Storage Materials, Media, and Systems
https://doi.org/10.52825/solarpaces.v1i.736

Published: 03 Jan. 2024

A Comparative Radiative Property Evaluation of Sintered Bauxite and AMS4003 Ceramic Particles

J. Michael Mayer[1][https://orcid.org/0000-0002-2275-9072], Brandon Surhigh[1][https://orcid.org/0000-0003-2528-5295], Kyu Bum Han[2][https://orcid.org/0000-0002-9505-2852], Eunjin Jeon[2], and Rohini Bala Chandran[1][https://orcid.org/0000-0002-2745-8893]

[1] University of Michigan, USA

[2] Advanced Materials Scientia LLC, USA

Abstract. The radiative properties of sintered bauxite (ACCUCAST ID80) and AMS4003 particles were measured and compared to assess their performances as direct absorption and heat transfer media for particle-based concentrated solar power (CSP) plants. Reflectance measurements were performed over the spectral range 0.2–20 μm and used to calculate solar and thermal emission properties of the particles. In addition, reflectance was measured as a function of temperature up to 1000 °C for the spectral range 1–20 μm. The solar absorptance of AMS4003 was greater than that of ACCUCAST both before and after thermal cycling of the materials at 1000 °C, although thermal cycling was found to substantially decrease the solar absorptance of both materials. The thermal emittance of AMS4003 was also greater than that of ACCUCAST at all temperatures tested. Finally, the radiaitve properties measured in this study were used to estimate absorber efficiencies as a way to compare the particles in terms of their performance in a solar receiver. AMS4003 yielded greater efficiencies than ACCUCAST, suggesting its potential as a material for CSP.

Keywords: CSP, Particles, Sintered Bauxite, Radiative Properties, Solar Absorptance, Thermal Emittance

1. Introduction

Ceramic particles are a promising candidate for next-generation CSP systems [1]. These systems will operate at high temperatures (> 700 °C) and utilize the particles as a direct absorption and heat transfer medium, including thermal energy storage (TES). At these high temperatures, radiation is a crucial mode of heat transfer and must be considered to accurately assess the performance of the particles. The operating temperature of the system is in part determined by the amount of solar energy absorbed by the particles and the amount of energy lost by the particles via thermal emission. In addition to being directly irradiated, the particles transfer heat through radiative exchange with their environment, surrounding components, and other particles in heat exchangers, storage bins, etc. These interactions cannot be quantified precisely without readily available radiative property data for the ceramic particles. In this study, the radiative properties of a commercially available sintered bauxite particle, ACCUCAST ID80 (CARBO Ceramics, Inc.), and AMS4003 (Advanced Materials Scientia, LLC), a novel, engineered ceramic particle, are characterized and compared in the solar and infrared wavelength ranges.

The radiative properties of sintered bauxite particles have been characterized by numerous studies in the solar and infrared spectra and as a function of temperature [2–9]. The most commonly studied particles are those produced by CARBO Ceramics, Inc., with product

names including ACCUCAST and CARBOHSP. These particles have been the focus of many studies because of their characteristics that make them suitable for CSP, including good durability, solar absorptance, and sphericity for ease of flow. Most studies aimed at characterizing the radiative behavior of these particles are concerned with their behavior in the visible and near-infrared wavelengths that are relevant to the solar spectrum. Several studies report solar absorptance values above 0.9, although thermal cycling is shown to decrease solar absorptance for CARBO and other sintered bauxite particles [2–5]. Notably, these studies do not measure the absorptance of the particles as a function of temperature, so solar absorptance is calculated using room-temperature data. Prior work has also been done to characterize sintered bauxite particles in the near- to mid-infrared wavelengths that are relevant to thermal emission [6–9]. This includes the use of emissometers to estimate thermal emittance at temperatures ≥ 700 °C with room-temperature measurements as well as temperature-dependent spectral emittance measurements. In this case, there is a larger spread in the data with thermal emittance, with values ranging from ~0.7 to ~0.95 at elevated temperatures. For AMS4003, there is currently no reported data available on its radiative properties. Therefore, the primary objective of this study is to experimentally determine radiative properties for AMS4003 and compare it against those measured for ACCUCAST ID80.

2. Methodology

2.1 Materials and Sample Preparation

The two particulate materials analyzed in this study are shown in Figure 1. ACCUCAST ID80 (Figure 1a) is a sintered bauxite particle with a reported composition largely consisting of alumina (70–80%), followed by silica (10–20%), iron oxide (5–10%), and titanium dioxide (1–5%). Due to the range in composition, two different batches of particles may exhibit slightly differently properties. Most ACCUCAST particles have a size between 100 and 200 μm. The composition of the AMS4003 particles (Figure 1b) is not currently disclosed. Most AMS4003 particles have a size between 200 and 400 μm.

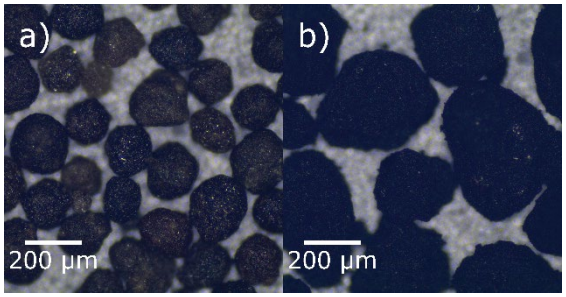

Figure 1. Microscope images of a) ACCUCAST ID80 and b) AMS4003 at 5x magnification.

Before making reflectance measurements, the particle size of both materials is reduced through a grinding and sieving process. This step is performed to prepare the material for diffuse reflectance spectroscopy, which is most reproducible for particle sizes less than 25 μm [10]. A 20 μm sieve is used to filter the particle size after grinding, and previous testing showed that this procedure does not discernably alter the composition of ACCUCAST [9].

The effects of thermal cycling were examined by placing the materials in a tube furnace at 500 °C and 1000 °C for 6 hours. While the particles would normally be at elevated temperatures for long durations in a CSP plant, longer cycling times like 12 hours did not produce further changes in the radiative behavior of the materials. It was found that the most important factor in the extent of thermal aging is the maximum temperature experienced by the particles. Additionally, it is hypothesized that the particle size reduction step accelerates the changes observed due to thermal cycling.

2.2 Diffuse Reflectance Spectroscopy

A well-established technique for characterizing the radiative behavior of powders or particulate media is diffuse reflectance spectroscopy (DRS). For data collection in the infrared wavelengths (1–20 μm), diffuse reflectance is measured with a specialized accessory (DiffusIR, PIKE Technologies) coupled with a Fourier transform infrared spectrometer, or FTIR (Nicolet iS50, Thermo Fisher Scientific). A UV–Vis spectrophotometer (UV-2600, Shimadzu Corp.) is used to collect reflectance data for wavelengths less than 1 μm. Reflectance R_λ is calculated as a ratio of intensities between the sample material being measured and a background material. The background material used for infrared DRS measurements is KBr powder, and the background material used for measurements in the UV–Vis is $BaSO_4$ powder. The background materials scatter incoming radiation with nearly no absorption. The powdered sample is estimated to be optically thick enough to assume negligibly small transmittance. Therefore, any radiation that is not absorbed is reflected. In addition, absorptance of the sample is considered a directionally-independent quantity because of the diffuse nature of the surface. Therefore, from Kirchoff's law, spectral emittance ε_λ and absorptance α_λ may be approximated for a diffuse sample as:

$$\varepsilon_\lambda = \alpha_\lambda = 1 - R_\lambda \tag{1}$$

Temperature-dependent reflectance data is collected with a heated stage accessory that heats the sample inside an alumina sample cup up to temperatures of 1000 °C. The measurement must be performed in vacuum to prevent heating of the window that covers the sample and significant heat losses due to natural convection. This capability was only available for the FTIR measurements; consequently, temperature-dependent reflectance is only reported for the infrared wavelengths (1–20 μm).

2.3 Data Processing

Spectral emittance data is transformed into a thermal emittance ε_{th} at a given temperature by normalizing emission from the sample with blackbody emission $E_{b\lambda}$:

$$\varepsilon_{th} = \frac{\int_0^\infty \varepsilon_\lambda E_{b\lambda}\, d\lambda}{\int_0^\infty E_{b\lambda}\, d\lambda} \tag{2}$$

Spectral emittance ε_λ is derived from the experimental reflectance data according to Eq. 1. Because the spectral range of measurement is limited to 1–20 μm for the temperature-dependent measurements, the integrals in Eq. 2 are only evaluated over this range. For temperatures such as 1000 °C, this is a fine approximation because ~99% of blackbody emissive power falls in this range. However at 100 °C, this range contains only ~83% of blackbody emissive power. Therefore, there is greater uncertainty in the thermal emittance calculation at lower temperatures, especially for temperatures < 400 °C.

Similarly, solar absorptance α_s is calculated by normalizing absorptance by the sample with the AM1.5D (direct normal) solar spectrum G_λ:

$$\alpha_s = \frac{\int_0^\infty \alpha_\lambda G_\lambda\, d\lambda}{\int_0^\infty G_\lambda\, d\lambda} \tag{3}$$

Spectral absorptance α_λ is derived from the experimental reflectance data according to Eq. 1. This quantity is calculated as independent of temperature due to experimental limitations with the UV–Vis spectrophotometer. The spectral range of measurement at room temperature (0.2–20 μm) contains essentially all of the incident solar spectrum.

To compare and evaluate the performance of the different materials, the radiative properties of the particles are used to calculate a solar-to-thermal absorber efficiency η_{abs}:

$$\eta_{abs} = \alpha_s - \frac{\varepsilon_{th}\sigma T^4}{CI} \quad (4)$$

Eq. 4 is a simplified calculation of the absorber efficiency of a concentrating solar receiver operating with a concentration ratio C, solar flux I, and uniform temperature T. Only radiative losses are modeled for simplicity, as they would dominate at elevated temperatures. In reality, other heat losses will be present in the system.

3. Results

3.1 Room-Temperature Measurements – Solar Absorptance

Figure 2 shows reflectance data for ACCUCAST ID80 and AMS4003 measured at room temperature before and after thermal cycling. The dotted lines represent data collected by the UV–Vis (0.2–1 µm), and the solid lines represent data collected by the FTIR (1–20 µm). There is a discontinuity in the reflectance data at 1 µm due to the change in instrumentation, which adds uncertainty to the calculated solar absorptance values. Differences may be caused by the use of different background materials for the different spectral regions, although there is continuity in the trends observed at 1 µm. The pre-thermal cycling results in Figure 2a show that AMS4003 is more absorbing in the solar spectrum (0.3–2.5 µm). This results in AMS4003 having a greater solar absorptance (0.94) as compared to ACCUCAST (0.69). Figure 2a also shows that ACCUCAST is significantly more reflective (less absorbing) in the infrared wavelengths 2.5–8 µm, including a peak reflectance of 73% at 4.6 µm. For longer wavelengths (> 8 µm), both materials exhibit low values of reflectance (< 14%).

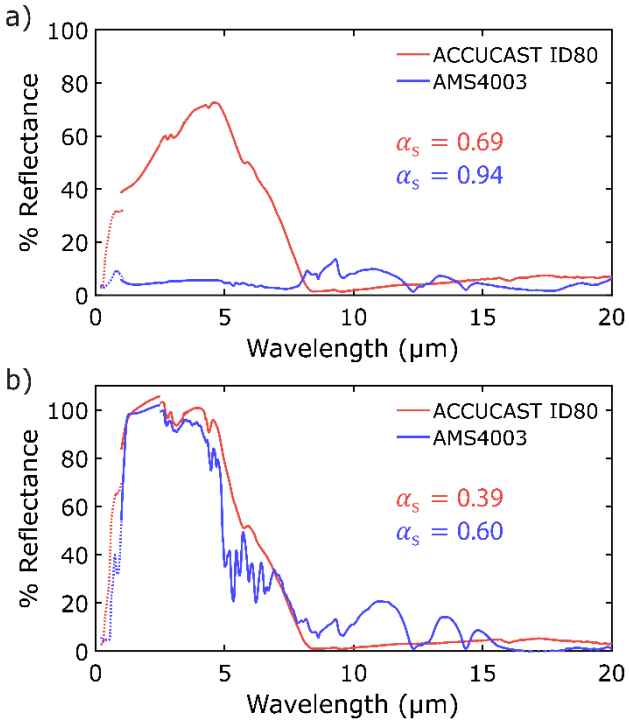

Figure 2. Room-temperature diffuse reflectance spectra for ACCUCAST ID80 and AMS4003 for a spectral range of 0.2–20 µm a) before and b) after thermal cycling at 1000 °C.

Figure 2b shows reflectance data for ACCUCAST ID80 and AMS4003 after the materials were thermally cycled at 1000 °C in air. Thermal cycling caused significant increases in reflectance in the visible and infrared wavelengths for both materials, and this reduced the solar absorptance of ACCUCAST to 0.39 and AMS4003 to 0.60. The mid-infrared (> 8 μm) spectral features were less affected by exposure to high temperatures, particularly for ACCUCAST. Microscope images for each material before and after thermal cycling at 500 °C and 1000 °C are shown in Figure 3. The images show that ACCUCAST and AMS4003 transition from a dark gray or black color to a dark orange or red color, which is responsible for the decrease in solar absorptance. Based on the composition of ACCUCAST, the change in color and radiative properties after heating is attributed to iron oxide [4,9].

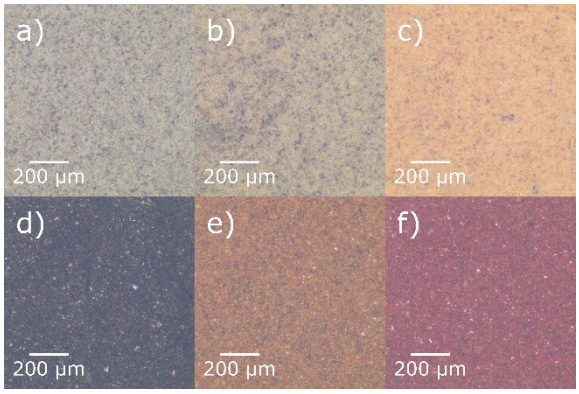

Figure 3. Microscope images of ACCUCAST ID80 a) before thermal cycling and after thermal cycling at b) 500 °C and c) 1000 °C; AMS4003 d) before thermal cycling and after thermal cycling at e) 500 °C and f) 1000 °C at 5x magnification.

3.2 Temperature-Dependent Measurements – Thermal Emittance

Figure 4 shows reflectance data for ACCUCAST ID80 and AMS4003 measured as a function of temperature up to 1000 °C. All data was collected with the heated stage accessory and FTIR (1–20 μm). It is important to note that the temperature-dependent reflectance data is acquired in vacuum, which means the oxidation-driven changes in color and radiative properties seen in the thermal cycling tests (Figures 2 and 3) are not equivalent to those of the heated stage. Temperature-dependent measurements show a general trend of decreasing reflectance (and therefore increasing emittance) with temperature for both materials. Temperature has the largest effect on ACCUCAST in the near-IR with the largest drop in reflectance occurring around 4.7 μm. For longer wavelengths (> 8 μm), the effect of temperature on reflectance is minimal because most of the radiation is absorbed at these wavelengths. AMS4003 exhibits a consistent decrease in reflectance with temperature over most of the measured spectrum, including a decrease of ~9% reflectance at 9.3 μm from 25 °C to 1000 °C. In general, the effect of temperature on the radiative behavior of AMS4003 is not nearly as pronounced as with ACCUCAST because AMS4003 is already quite absorptive, especially in the near-IR.

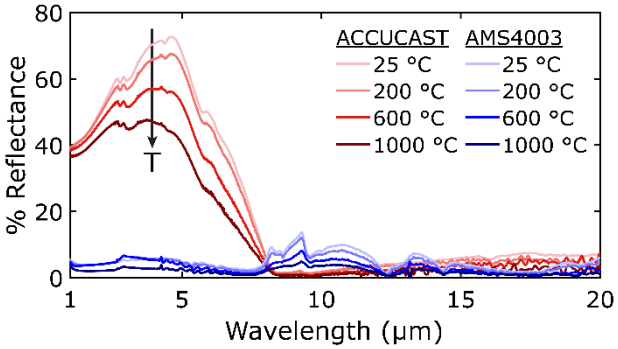

Figure 4. Temperature-dependent diffuse reflectance spectra for ACCUCAST ID80 and AMS4003 from 25 °C to 1000 °C for a spectral range of 1–20 μm.

Figure 5 shows thermal emittance calculated using the temperature-dependent reflectance data and Eq. 2. Both materials exhibit high thermal emittance (> 0.9) at room temperature. The major difference observed between the two materials is that ACCUCAST shows a decreasing thermal emittance with temperature, whereas thermal emittance increases marginally with temperature for AMS4003. The behavior of thermal emittance is dictated by two competing effects—the spectral weighting of the blackbody function at a given temperature and the temperature-dependent spectral emittance. At higher temperatures, the blackbody emission spectrum is shifted towards shorter wavelengths. In the case of ACCUCAST, the blackbody spectrum is weighting parts of the spectrum with higher reflectance (lower emittance) as temperature increases. This leads to a decreasing thermal emittance with temperature. However, the spectral emittance is also increasing with temperature, and this effect is significant enough at higher temperatures (> 600 °C) to prevent further decreases in thermal emittance with temperature. In the case of AMS4003, the strong absorption behavior across the spectrum results in thermal emittance values > 0.94 for all temperatures.

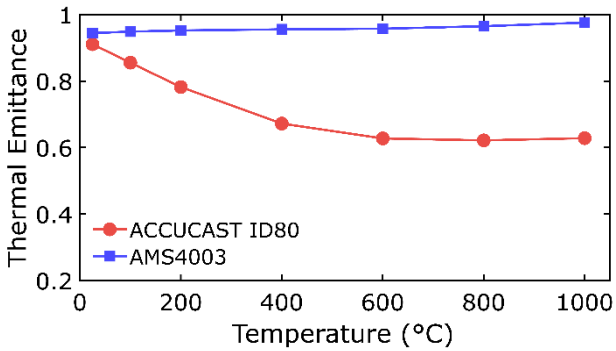

Figure 5. Calculated thermal emittance for ACCUCAST ID80 and AMS4003 up to 1000 °C.

Absorber efficiencies for different concentration ratios and receiver temperatures are shown in Figure 6. It is assumed that the incident solar flux is 1 sun (1000 W/m^2). It is also assumed that solar absorptance is independent of temperature. The efficiency values are calculated using the solar absorptance of the materials after thermal cycling (Figure 2b) and their temperature-dependent thermal emittance (Figure 4). For nearly all combinations of temperature and concentration shown in Figure 6, AMS4003 demonstrates superior absorber efficiency; this is a direct result of its higher solar absorptance. However, the higher thermal emittance of AMS4003 means that as temperatures continue to increase, the absorber efficiency of ACCUCAST will eventually become larger. This is true especially at lower concentrations where the effect of thermal emission losses are more significant. For example, at a concentration of 250 suns, the difference in absorber efficiency between ACCUCAST and AMS4003 at 400 °C is 0.19. At 1000 °C, the efficiencies are approximately equal.

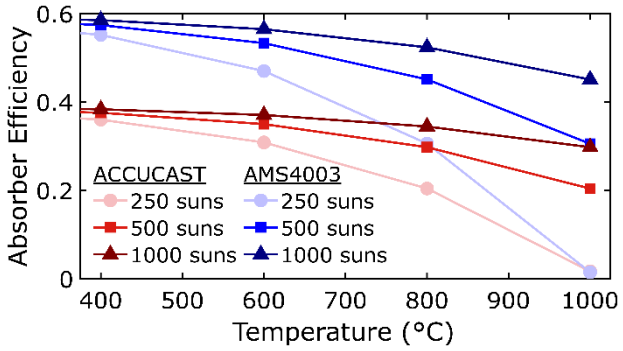

Figure 6. Calculated absorber efficiencies for ACCUCAST ID80 and AMS4003 from 400 °C to 1000 °C for concentration ratios of 250, 500, and 1000 suns.

4. Summary and Conclusions

The radiative properties of two ceramic particles, ACCUCAST ID80 and AMS4003, were evaluated and compared in the context of particle-based CSP. Spectroscopic measurements were taken over a spectral range of 0.2–20 μm to calculate reflectance, and spectral reflectance values were used to derive the solar absorptance and thermal emittance of the particles. The solar absorptance of AMS4003 was higher than that of ACCUCAST both before and after thermal cycling at 1000 °C. Thermal cycling in air proved to significantly decrease the solar absorptance of both materials, which was observed as a noticeable change in the color of the particles from black and dark gray to reddish-orange. Temperature-dependent reflectance was measured over the range 1–20 μm. These values were used to calculate thermal emittance as a function of temperature, and it was shown that the thermal emittance of ACCUCAST decreases with temperature up to 600 °C before stabilizing at a value of ~0.6. In contrast, the thermal emittance of AMS4003 is consistently above 0.9 and even increases with temperature. Finally, solar absorptance and temperature-dependent thermal emittance values were used to calculate absorber efficiency values. AMS4003 exhibited greater efficiency than ACCUCAST in the temperature range 400–1000 °C and concentration ratio range 250–1000 suns, despite its greater thermal emittance at these temperatures. These results indicate that AMS4003 is a potentially promising candidate for increasing efficiency in solar receivers in CSP plants.

Data Availability Statement

The data that support the findings of this study are available from the corresponding author (J.M. Mayer) upon reasonable request.

Author Contributions

J. Michael Mayer: conceptualization, data curation, formal analysis, investigation, methodology, visualization, writing – original draft, writing – review & editing. **Brandon Surhigh**: data curation, investigation, methodology. **Kyu Bum Han**: conceptualization, investigation, resources, writing – review & editing. **Eunjin Jeon**: investigation, resources. **Rohini Bala Chandran**: conceptualization, formal analysis, funding acquisition, supervision, writing – review & editing.

Competing Interests

The authors declare no competing interests.

Funding

This work was supported by the U.S. Department of Energy's Office of Energy Efficiency and Renewable Energy (EERE) under the Solar Energy Technologies Office (SETO) award number DE-EE0009819. The authors also acknowledge the financial support provided by startup funds from the Department of Mechanical Engineering and the College of Engineering at the University of Michigan.

References

1. C. K. Ho, K.J. Albrecht, L. Yue, B. Mills, J. Sment, J. Christian, and M. Carlson, "Overview and design basis for the Gen 3 Particle Pilot Plant (G3P3)," *AIP Conf. Proc.*, vol. 2303, no. 1, Dec. 2020, Art no. 030020, doi: https://doi.org/10.1063/5.0029216.
2. K.A. Stahl, J.W. Griffin, and R.B. Pettit, "Optical properties of solid particle receiver materials: II. Diffuse reflectance of Norton Masterbeads at elevated temperatures," *Sol. Energy Mater.* vol. 14, no. 3–5, pp. 417–425, Nov. 1986, doi: https://doi.org/10.1016/0165-1633(86)90063-8.
3. J. Roop, S. Jeter, S.I. Abdel-Khalik, and C.K. Ho, "Optical properties of select particulates after high-temperature exposure," *Proc. 8th Int. Conf. Energy Sustain.*, Oct. 2014, Art no. ES2014-6504, V001T02A029, doi: https://doi.org/10.1115/ES2014-6504.
4. N.P. Siegel, M.D. Gross, and R. Coury, "The Development of Direct Absorption and Storage Media for Falling Particle Solar Central Receivers," *J. Sol. Energy Eng.*, vol. 137, no. 4, Aug. 2015, Art no. 041003, doi: https://doi.org/10.1115/1.4030069.
5. B. Gobereit, L. Amsbeck, C. Happich, and M. Schmücker, "Assessment and improvement of optical properties of particles for solid particle receiver," *Sol. Energy.*, vol. 199, pp. 844–851, Mar. 2020, doi: https://doi.org/10.1016/j.solener.2020.02.076.
6. N. Schroeder and K. Albrecht, "Assessment of particle candidates for falling particle receiver applications through irradiance and thermal cycling," *Proc. 15th Int. Conf. Energy Sustain.*, Jul. 2021, Art no. ES2021-62305, V001T02A003, doi: https://doi.org/10.1115/ES2021-62305.
7. J. Chen, J.F.Torres, S. Hosseini, A. Kumar, J. Coventry, and W. Lipiński, "High-temperature optical and radiative properties of alumina–silica-based ceramic materials for solar thermal applications," *Sol. Energy Mater. Sol. Cells.* vol. 242, Aug. 2022, Art no. 111710, doi: https://doi.org/10.1016/j.solmat.2022.111710.
8. C. Chen, C. Yang, K. Pan, D. Ranjan, P.G. Loutzenhiser, and Z.M. Zhang, "Temperature-dependent spectral emittance of bauxite and silica particle beds," *Exp. Heat Transf.*, May 2022, doi: https://doi.org/10.1080/08916152.2022.2080301.
9. J. M. Mayer, J.A. Abraham, B. Surhigh, B. Kinzer, and R. Bala Chandran, "Temperature-dependent diffuse reflectance measurements of ceramic powders in the near- and mid-infrared spectra," *Sol. Energy.*, vol. 245, pp. 193–210, Oct. 2022, doi: https://doi.org/10.1016/j.solener.2022.08.071.
10. O. Faix and J.H. Böttcher, "The influence of particle size and concentration in transmission and diffuse reflectance spectroscopy of wood," *Holz als Roh- und Werkst.* vol. 50, pp. 221–226, Jun. 1992, doi: https://doi.org/10.1007/BF02650312.